

1 Wall loss of semi-volatile organic compounds in a Teflon bag chamber 2 for the temperature range of 262-298 K: mechanistic insight on 3 temperature dependence

4 Longkun He¹, Wenli Liu², Yatai Li^{1,3}, Jixuan Wang¹, Mikinori Kuwata², Yingjun Liu¹

5 ¹State Key Joint Laboratory of Environmental Simulation and Pollution Control, College of Environmental Sciences and
6 Engineering, Peking University, Beijing, 100871, China

7 ²Department of Atmospheric and Oceanic Sciences and Laboratory for Climate and Ocean-Atmosphere Studies, School of
8 Physics, Peking University, Beijing 100871, China

9 ³Now at College of Public Health, Zhengzhou University, Zhengzhou, 450001, China

10 Correspondence to: Mikinori Kuwata (kuwata@pku.edu.cn), Yingjun Liu (yingjun.liu@pku.edu.cn)

11
12 **Abstract.** Teflon bag chambers have long been used for investigating atmospheric chemical processes, including secondary
13 organic aerosol formation. ~~The w~~Wall-loss process of gas-phase species in Teflon bag chambers has typically been investigated
14 at around room temperature. Recent laboratory studies started employing Teflon bag chambers at sub-273 K conditions for
15 simulating wintertime and upper tropospheric environments. However, temperature dependence in vapor wall-loss processes
16 of semi-volatile organic compounds (SVOCs) in a Teflon bag chamber has not well been investigated. In this study, we
17 experimentally investigated wall-loss process of C₁₄-C₁₉ *n*-alkanes in a 1 m³ Teflon bag for the temperature range of 262 to
18 298 K. Enhanced wall losses of the tested *n*-alkanes were observed following the decrease in temperature. For instance, 65%
19 of C₁₄ *n*-alkane was lost to the wall 15 hours after injection at room temperature, while the corresponding value was 95% at
20 262 K. The experimental data were analyzed using the two-layer kinetic model, which considers both absorption of gas phase
21 species to the surface layer of Teflon wall and diffusion to the inner layer. The experimental data demonstrated that absorption
22 of gas phase species by the surface layer enhanced at lower temperature. The temperature dependence in absorption was well
23 accounted using the equilibrium dissolution model of organic compounds to the Teflon surface by considering reduced
24 saturation vapor pressure at lower temperature. On the contrary, diffusion ~~process~~ of *n*-alkanes from the surface to inner layer
25 slowed down at reduced temperature. ~~Hence the relative importance of the surface and inner layers on wall loss process~~
26 ~~changes with temperature.~~ Mechanistic studies on these processes will need to be conducted in the future to quantitatively
27 predict the influence of temperature-dependent wall-loss processes of SVOCs on laboratory experimental results.

28 **1 Introduction**

29 The environmental chamber is one of the most widely-used laboratory systems for studying chemical processes in
30 the atmosphere, including formation of secondary organic aerosol (SOA) (Clark et al., 2016; Nakao et al., 2011; Ng et al.,
31 2007; Song et al., 2005). The environmental chambers are typically made of Teflon films or stainless steel (Cocker et al., 2001;
32 Bunz et al., 1996; Voigtlaender et al., 2012). Existence of walls in the environmental chambers induces losses of both vapors
33 and particles due to their deposition on wall surfaces (McMurry and Grosjean, 1985; Krechmer et al., 2020). Wall loss of gas-
34 phase organic compounds in the environmental chambers can lead to underestimation of SOA mass yields. For instance,
35 injection of seed particles into Teflon bag has been shown to increase SOA yields by a few times due to the reduced relative
36 importance of the chamber wall as a condensation sink in the system (Kroll et al., 2007; Zhang et al., 2014).

37 Vapor wall loss in Teflon bag chambers, especially that for semi-volatile organic compounds (SVOCs), has been
38 intensively investigated in the last decade (Matsunaga and Ziemann, 2010; Yeh and Ziemann, 2014, 2015; Zhang et al., 2015;
39 Krechmer et al., 2016; Huang et al., 2018b; Pratap et al., 2020; Yu et al., 2022). For instance, Matsunaga and Ziemann (2010)
40 studied wall-loss process of alkanes, alkenes, alcohols, and ketones. These previous wall-loss experiments were dominantly
41 conducted at around room temperature (293~303 K), as most of the chamber studies employed the corresponding temperature
42 range (Hidy, 2019). The experimental results were often modeled by assuming equilibrium dissolution of the organic
43 compounds into the Teflon film. A more recent study separately considered the surface and inner layer of the Teflon film for
44 explaining the loss process more quantitatively (Huang et al., 2018b).

45 Recently, a growing number of environmental chamber experiments have been conducted at low temperatures to
46 simulate wintertime/upper tropospheric conditions in laboratory (Huang et al., 2018a; Pratap et al., 2019; Quelever et al., 2019;
47 Simon et al., 2020; Wang et al., 2022). For instance, some SOA formation experiments have been conducted for the
48 temperature range down to 223 K using stainless steel chambers such as the Aerosol Interaction and Dynamics in the
49 Atmosphere (AIDA) and Cosmics Leaving Outdoor Droplets (CLOUD) chambers (Huang et al., 2018a; Simon et al., 2020).
50 Teflon bag chambers have also been employed for the temperature range down to 258 K (Kristensen et al., 2017; Deng et al.,
51 2021). These studies demonstrate that temperature is an important parameter determining both mass yields and chemical
52 composition of SOA. Vapor wall loss of SVOCs in the environmental chambers for the corresponding temperature range needs
53 to be understood for better interpreting these experimental data in a quantitative way. So far only one group attempted to
54 investigate vapor wall loss below room temperature, by measuring the size evolution of levoglucosan particles injected into a
55 Teflon chamber (Pratap et al., 2020). However, the experimental results were confounded by slow evaporation of levoglucosan
56 from particles at low temperatures.

57 This study investigated vapor wall loss of C₁₄-C₁₉ *n*-alkanes in a Teflon chamber for the temperature range of 262 to
58 298 K by monitoring the evolution of their gas-phase concentrations following a pulse release. The wall-loss process was

59 investigated as a function of temperature. The experimental results were analyzed using the two-layer kinetic model, which
60 considers partitioning of gas phase SVOCs to the surface layer, as well as further diffusion to the inner layer. Temperature
61 effects on the two processes were evaluated separately.

62 **2 Experimental**

63 **2.1 Teflon chamber experiments**

64 Figure 1 shows the experimental setup. The experiment was conducted using a fluorinated ethylene propylene (FEP)
65 bag with the volume of 1 m³. The thickness of the FEP film for the bag was 75 μm. The dimension of the bag was 260 cm ×
66 55 cm × 70 cm. The area to volume ratio of the chamber was 7.26 m⁻¹. The chamber volume was experimentally validated by
67 employing CO₂ as a tracer (Figure S1). The timescale for CO₂ to be well mixed in the bag after a pulse injection was
68 approximately 30 mins (Figure S1). The bag was newly purchased for the experiment, meaning that it was employed for no
69 other experiments. The bag was installed in a chest freezer (Type 2288, Nixue Inc.), which was equipped with an additional
70 internal thermal insulation layer. Two fans were installed in the freezer (outside the bag) to ~~promote the~~ facilitate mixing of ~~the~~
71 air so that air temperature in the freezer was uniform. The temperature of the freezer was measured at 3 points using temperature
72 sensors (Figure 1). Temporal variation of temperature was ± 0.5 K at 262 K.

73 Throughout the experiments, purified air was employed. The purified air was produced using a zero air generator
74 (Model 747–30, AADCO Instruments, Inc.) and further purified using a hydrocarbon trap (BHT-2, Agilent Technologies, Inc.).
75 Hydrocarbon concentration in the purified air was less than 5 ppbv. Relative humidity (RH) was less than 0.1%.

76 Solutions containing C₁₄ - C₁₉ *n*-alkanes (Konoscience Inc., > 98%) were prepared and injected into the chamber.
77 Hexane (Fisher Chemical Co., HPLC grade) was employed as the solvent. The purities and saturation vapor pressures of all
78 chemicals are given in Table S1. The solutions were injected to the chamber using a syringe pump (Fusion 200 Touch, Chemyx
79 Inc.) and a nebulizer (TR-30-A1, Meinhard Inc.) through polytetrafluoroethylene (PTFE) tubing, as shown in Figure 1. The
80 use of nebulizer expedited the evaporation of the solution.

81 Eight sets of wall-loss experiments were conducted in the temperature range of 262 to 298 K. Prior to each experiment,
82 the chamber was heated to ~320 K and continuously flushed using purified air. The cleaning process lasted for 2~3 days until
83 the concentration of investigated *n*-alkanes dropped to the background level. To start an experiment, the chamber was switched
84 to batch mode and the solution was injected to the chamber at room temperature. The injection lasted for 13 mins, with a liquid
85 flow rate of 100 μL min⁻¹. The air flow rate of the nebulizer was 0.7 L min⁻¹. The resulting initial concentrations (*C*₀) of
86 individual *n*-alkanes in the chamber ranged from 4 to 50 μg m⁻³ assuming no wall loss, which were lower than 20% of their
87 saturation concentrations under the corresponding experimental temperature to avoid particle formation. The solution used for
88 low-temperature experiments (< 278 K) did not contain C₁₈ and C₁₉ *n*-alkanes to avoid formation of particles. For experiments

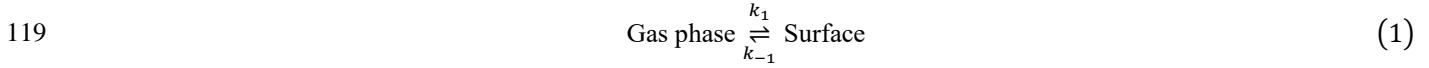
89 below room temperature, the cooling system of the freezer was turned on one hour after the completion of the injection. The
90 operation procedure was employed to avoid homogeneous nucleation and subsequent condensational growth of aerosol
91 particles. The validity of employing this post-cooled operation procedure was demonstrated by comparison with a pre-cooled
92 chamber result at 270 K (Figure S2). Measurements using an optical particle counter (11-D, GRIMM Aerosol Technik Ainring,
93 Germany) experimentally confirmed negligible abundance of aerosol particles in the chamber ($< 0.5 \mu\text{g m}^{-3}$). It took ~ 3 hours
94 for the temperature in the freezer to drop to a stable level after injection (Figure S2S3). Although the air in the bag leaked out
95 during experiments due to compression of the bag by its own weight, absence of intrusion of room air to the bag was confirmed
96 by observing no changes in contaminant signals (Table S2). The gas-phase concentrations of *n*-alkanes were therefore
97 unaffected by the changes in bag volume.

98 Concentrations of SVOCs in the chamber were quantified using the semi-volatile thermal desorption aerosol gas
99 chromatograph (SV-TAG, Aerodyne Research Inc. & Aerosol Dynamic Inc., USA) (Zhao et al., 2013). The gas
100 chromatography-mass spectrometer (GC-MS) (7890B, Agilent Technologies, Inc.) was employed for the system. Detailed
101 descriptions of the SV-TAG operation and performance tests were presented in our previous papers (Li et al., 2022a; Li et al.,
102 2022b). Herein, chamber air was sampled through ~ 1 m long perfluoroalkoxy alkane (PFA) tubing (1/4 inch in diameter). Prior
103 to sampling, the chamber air passed through the PFA tubing at 0.5 L min^{-1} for at least 20 min for passivating the tubing wall
104 (Matsunaga and Ziemann, 2010). Samples were periodically collected for 5 min at 4 L min^{-1} for each time at 1-15 hours after
105 injection. As the absence of particles was confirmed, only gas-phase SVOCs were sampled by the SV-TAG. The instrument
106 response to *n*-alkanes was calibrated with standards before and after each experiment (Figure S3S4), utilizing the in-situ
107 automatic injection system (Isaacman et al., 2011). The gas-phase concentrations of SVOCs were calculated from the measured
108 quantity of SVOCs and sampled air volume.

109 2.2 Kinetic model

110 Herein we used a unified vapor wall-loss transport model developed by Huang et al. (2018b) to fit the experimental
111 data. Figure 2 shows the concept of the model. Briefly, SVOCs partition between the gas phase and the surface of the FEP
112 film. Subsequently, the absorbed SVOCs may diffuse to the inner layer of the film. As the thickness of the FEP film (75 μm)
113 is a couple of orders larger than that of the surface layer ($\sim 5 \text{ nm}$) (Huang et al., 2018b), the inner layer is assumed as an
114 infinite sink. As a result, the diffusion process of SVOCs from the inner layer to the film surface is ignored. A list of all the
115 parameters is provided in Nomenclature. The governing equations without and with considering diffusion to the inner layer
116 are presented below, respectively.

117 (1) Without considering the diffusion process in the inner layer, the wall loss process is solely controlled by
118 partitioning of SVOCs between the gas phase and surface layer and can be described as follows



120 where k_1 and k_{-1} are forward and backward rate constants in the process. The corresponding first-order kinetic equations are

121
$$\begin{aligned} \frac{dC_{gas}}{dt} &= -k_1 C_{gas} + k_{-1} C_{surface} \\ \frac{dC_{surface}}{dt} &= k_1 C_{gas} - k_{-1} C_{surface} \end{aligned} \quad (2)$$

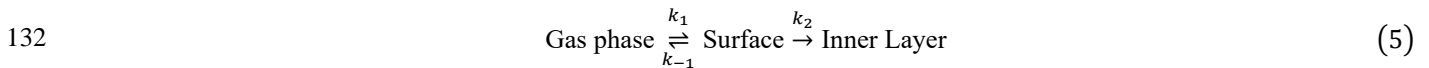
122 where C_{gas} and $C_{surface}$ are the SVOC concentrations in gas phase and on wall surface, respectively. It should be noted that
 123 $C_{surface}$ was defined as the total mass of SVOC that was divided by the chamber volume, following previous studies
 124 (Matsunaga and Ziemann, 2010; Yeh and Ziemann, 2014, 2015). This model has been commonly used to interpret the
 125 experimental data of vapor wall loss in previous studies (Matsunaga and Ziemann, 2010; Yeh and Ziemann, 2014, 2015;
 126 Zhang et al., 2015).

127 The gas-surface equilibrium time scale $\tau_{surface}$ and equilibrium constant K_{eq} can be obtained by

128
$$\tau_{surface} = \frac{1}{k_1 + k_{-1}} \quad (3)$$

129
$$K_{eq} = \frac{k_1}{k_{-1}} = \left[\frac{C_{surface}}{C_{gas}} \right]_{eq} \quad (4)$$

130 (2) Considering the diffusion process in the inner layer, the whole vapor wall loss process can be formulated as
 131 follows



133 where k_2 is the first-order loss rate constant in the diffusion process. Correspondingly, the kinetic processes for C_{gas} and
 134 $C_{surface}$ can be described by the following equations

135
$$\begin{aligned} \frac{dC_{gas}}{dt} &= -k_1 C_{gas} + k_{-1} C_{surface} \\ \frac{dC_{surface}}{dt} &= k_1 C_{gas} - k_{-1} C_{surface} - k_2 C_{surface} \end{aligned} \quad (6)$$

136 The diffusion process has the first-order decay time scale τ_{inner} of $\tau_{inner} = \frac{1}{k_2}$. If $k_2 \ll k_1 + k_{-1}$ (i.e., $\tau_{inner} \gg \tau_{surface}$),
137 gas-surface partitioning occurs much faster than the diffusion process to the inner layer. In this case, the apparent first-order
138 decay loss constant ~~the loss rate~~ of SVOC from the gas phase can asymptotically be represented as (Huang et al., 2018b):

$$139 \quad \frac{dC_{gas}}{C_{gas}dt} \approx -\frac{K_{eq}}{1 + K_{eq}}k_2 \quad (7)$$

140 The data analysis and model fitting were conducted using Wolfram Mathematica 13.1. The controlling factors of
141 individual parameters in the above equations were previously discussed by Huang et al. (2018b).

142 **3 Results and discussion**

143 **3.1 Wall loss of *n*-alkanes at room temperature**

144 An example of temporal profile for C₁₄-C₁₉ *n*-alkanes during the experiment at 298 K is shown in Figure 3. The figure
145 demonstrates the temporal change of C_{gas}/C_0 , where C_0 indicates the initial concentration of *n*-alkanes. The values of C_{gas}/C_0
146 for each *n*-alkane exhibited similar patterns. During the first one hour following the injection, C_{gas}/C_0 exponentially decreased.
147 After that, gradual decreases in C_{gas}/C_0 were observed. For example, the decline in gas fraction for C₁₄ *n*-alkane during the
148 first hour accounted for 71% of the total change in C_{gas}/C_0 over the whole experimental period of 15 hours. The values of
149 C_{gas}/C_0 decreased with the increase in carbon number, indicating enhanced wall loss. The values of C_{gas}/C_0 at 15 hours after
150 injection were 0.32, 0.25, 0.16, 0.097, 0.069, and 0.037 for C₁₄ - C₁₉ *n*-alkanes, respectively.

151 The experimental result can be well fitted using the two-layer model, but the fits deteriorate in the case that diffusion
152 in the inner layer is neglected (Figure 3). The optimized parameter sets are shown in Table S3. Mass fractions of injected
153 chemical species in the gas, surface, and inner layer phases that were estimated using the model are shown in Figure S4S5. In
154 the case of the most volatile compound (C₁₄ *n*-alkane), the maximum mass fraction in the surface phase occurred at 2 hours
155 after injection. Subsequently, the mass fractions for the compound in both gas phase and surface layer gradually decreased.
156 During this period, the ratio of the mass in the surface layer to that in the gas phase stabilized at 1.33. The mass fraction of the
157 compound in the inner layer steadily increased, reaching 0.22 at 15 hours after injection.

158 In the case of the least volatile compound (C₁₉ *n*-alkane), the mass fraction in the surface layer reached the maximum
159 (~76%) approximately 1 hour after injection, accounting for the rapid decrease in the observed concentration in the gas phase.
160 Subsequently, mass fractions of the compound in the gas phase and in the surface layer decreased in proportion. The
161 concentration ratio of the gas phase and surface later was maintained as a constant ~~maintaining a constant ratio of the two~~

162 (Figure S4S5). The mass fraction of the compound in the inner layer kept increasing during the experiment. At 15 hours after
163 injection, 87% of the compound existed in the inner layer.

164 The time scale for *n*-alkanes to reach partitioning equilibrium between the gas and surface phases is estimated to be
165 12 ~ 35 mins, consistent with literature data. For example, Matsunaga and Ziemann (2010) reported that the corresponding
166 time scale for C₈ - C₁₆ alkanes was 60 ± 20 mins. The corresponding value for oxygenated organic compounds was reported
167 as 26 ± 23 mins (Yeh and Ziemann, 2015).

168 Our result for the mass transfer of SVOCs to the inner layer can also be compared with a previous study. The rates
169 for the decrease in C_{gas}/C_0 for C₁₄-C₁₉ *n*-alkanes were 0.6–1.3% hour⁻¹ after the partitioning between gas phase and surface
170 layer reached equilibrium (*i.e.*, 3 ~ 15 hours). Yeh and Ziemann (2015) reported the corresponding value for 2-ketones as
171 approximately 1% hour⁻¹ for the time scale of 7 hours. They suggested that the value is close to the theoretical value for the
172 Fickian diffusion loss rate (~0.5 % hour⁻¹).

173 3.2 Temperature dependence of wall loss of *n*-alkanes

174 Figure 4a summarizes the values of C_{gas}/C_0 for all experiments at 3 hours after injection. The data for this sampling
175 time was selected, as the loss of gas phase species by partitioning to the surface layer accounted for the dominant portion of
176 the decline in the gas phase concentration. It should be noted that fitting the experimental data using the two-layer model was
177 challenging for the low-temperature experiments. ~~Since the chamber was cooled after the injection of *n*-alkanes, the model~~
178 ~~parameters would change correspondingly with chamber temperature, as the chamber was cooled after the injection of *n*-~~
179 ~~alkanes.~~ Potential uncertainties associated with the employment of the data at 3 hours after injection as a proxy for gas-surface
180 partitioning are summarized in Text S1.

181 Generally, C_{gas}/C_0 was lower for less volatile compounds and at lower temperature, suggesting enhanced partitioning
182 of *n*-alkanes to the chamber wall. The data for the room temperature ($C_{gas}/C_0 = 0.47, 0.45, 0.34, 0.24, 0.17,$ and 0.091 for C₁₄,
183 C₁₅, C₁₆, C₁₇, C₁₈, and C₁₉ *n*-alkanes) were smaller than that have been reported by a previous study. Namely, Matsunaga and
184 Ziemann (2010) quantified the corresponding values for equilibration between the gas and surface phases for C₁₄-C₁₆ *n*-alkanes
185 as ~80 – 90%. The enhanced partitioning to the surface layer in our study is likely due to that the chamber ~~we used~~ for the
186 present study is smaller (1 m³ versus 5.9 m³) has a larger area to volume ratio (7.26 m⁻¹ versus 3.39 m⁻¹).

187 Figure 4b shows the values of C_{gas}/C_0 as a function of temperature at 15 hours after injection. In all experiments, the
188 values of C_{gas}/C_0 at 15 hours after injection were consistently lower than those for 3 hours. For instance, C_{gas}/C_0 for C₁₄ *n*-
189 alkane at 262 K decreased from 0.15 (3 hours) to 0.06 (15 hours). As discussed in the case of the experiment at 298 K, the
190 result suggests that diffusional loss in the inner layer of the chamber wall occurred for the whole temperature range.

191 3.3 Temperature dependence of partitioning between gas phase and wall surface

192 The temperature dependence in the data summarized in Figure 4a can be understood by considering changes in
193 partitioning between the gas phase and surface layer. Matsunaga and Ziemann (2010) introduced the following equation for
194 relating $C_{surface}/C_{gas}$ and temperature based on the equilibrium dissolution model:

$$195 \left[\frac{C_{surface}}{C_{gas}} \right]_{eq} = K_{eq} = \frac{C_{FEP_surface}RT}{M_{wall}\gamma_{FEP_surface}P_s(T)} \quad (8)$$

196 where $C_{FEP_surface}$ is the equivalent organic mass concentration of the FEP chamber surface wall, M_{wall} is the average
197 molecular mass of the FEP, $\gamma_{FEP_surface}$ is the activity coefficient of the organic compound in the Teflon surface, R is the gas
198 constant, and T is temperature. $P_s(T)$ is the saturation vapor pressure of the compound at temperature T . To use Equation (8)
199 $P_s(T)$ was calculated by the EVAPORATION group contribution method (Compernelle et al., 2011). Comparison between
200 the EVAPORATION method with other approaches for estimating $P_s(T)$ is available in Figure [SSS6](#). The value of
201 $[C_{surface}/C_{gas}]_{eq}$ was approximated using $1/[C_{gas}/C_0]_{at\ 3\ hours} - 1$ by assuming that diffusion of n -alkanes to the inner layer
202 was still a minor loss process within 3 hours. Among the terms for the right-hand-side of equation (8), $RT/P_s(T)$ can be
203 calculated from the experimental conditions. The equation suggests that $[C_{surface}/C_{gas}]_{eq}$ and $RT/P_s(T)$ may linearly
204 correlate with the slope of $C_{FEP_surface}/(M_{wall}\gamma_{FEP_surface})$.

205 Figure 5 shows the correlations between $C_{surface}/C_{gas}$ and $RT/P_s(T)$ for individual compounds. For all the tested
206 compounds, these two parameters correlated well, even though $C_{surface}/C_{gas}$ increased by more than one order of magnitude
207 when the chamber was cooled down. The result suggests that equation (8) can be applied to a wide range of temperatures
208 without considering the temperature dependence of $C_{FEP_surface}/(M_{wall}\gamma_{FEP_surface})$ to account for partitioning of [a chemical](#)
209 [species \$n\$ -alkanes](#) to the surface layer. In other word, $\gamma_{FEP_surface}$ can be practically treated as a constant for the investigated
210 temperature range, given $C_{FEP_surface}$ and M_{wall} are independent of temperature. This implication is consistent with previous
211 findings that the activity coefficients of organic compounds in polymers only change slightly with temperature. For instance,
212 Kontogeorgis et al. (1993) compared the experimental and modelled values of activity coefficients for hydrocarbons in a few
213 polymers such as low-density polyethylene. The values of activity coefficients change by 10~20% for a temperature change
214 of 100 K. [Further studies, that employ different chemical species, would be needed in the future for validating and applying](#)
215 [the relation to a wider range.](#)

216 Values of $\gamma_{FEP_surface}$ for n -alkanes can be estimated from Figure 5. Based on equation (8), the fitted slopes
217 correspond to $C_{FEP_surface}/(M_{wall}\gamma_{FEP_surface})$. For a specific chamber design, compound-independent $C_{FEP_surface}$ can be
218 estimated by the density of FEP film (2150 kg m^{-3}) and the thickness of surface layer ($\sim 5\text{ nm}$) (Huang et al., 2018b). For the

219 chamber in this experiment, $C_{FEP_surface}$ ~~was assumed as~~ 78.2 mg m⁻³, following the recommendation by Huang et al.
220 (2018b). For estimating compound-dependent $\gamma_{FEP_surface}$, previous studies assumed $M_{wall} = 200$ g mol⁻¹ (Huang et al., 2018b;
221 Matsunaga and Ziemann, 2010). The same approximations were employed in the present study.

222 Figure 6 plots the retrieved values of $\gamma_{FEP_surface}$ for *n*-alkanes against $P_s(298\text{ K})$ for *n*-alkanes. The figure also
223 shows the corresponding parameters obtained from previous experimental studies (compiled by Huang et al. (2018b), including
224 Matsunaga and Ziemann (2010), Yeh and Ziemann (2014, 2015), and Krechmer et al. (2016)). It should be noted that the
225 literature results were analyzed with fixed values of area to volume ratio of 3 m⁻¹ and $C_{FEP_surface}$ of 32.2 mg m⁻³ (Huang et
226 al., 2018b). Regardless of differences in types of chemicals and chambers, the experimentally estimated values of $\gamma_{FEP_surface}$
227 and $P_s(298\text{ K})$ correlate in logarithmic ~~axes~~ scale. The relationship followed the equation of $-\ln(\gamma_{FEP_surface}) = 0.40 -$
228 $0.61\ln(P_s(298\text{ K}))$.

229 3.4 Characterization of diffusion from the Teflon surface to inner layer

230 Values of k_2 were estimated using equation (7), since values of τ_{inner} are at least 18 times larger than those of
231 $\tau_{surface}$ (Table S3). The values of C_{gas}/C_0 at 3 hours after injection were employed to calculate K_{eq} as discussed earlier.
232 The experimental data for 9, 12, and 15 hours after injection was employed for obtaining k_2 .

233 Figure 7 plots the estimated values of k_2 against $P_s(T)$ for all compounds in all experiments. The values of k_2 and
234 $P_s(T)$ positively correlate. As a comparison point, a previous study reported positive correlations for (1) the diffusivity of
235 organic compounds in FEP film and saturation concentration, and (2) k_2 and diffusivity (Huang et al., 2018b). Our current
236 result is qualitatively similar to the previous study, though temperature was maintained as a constant in the previous study.
237 The decrease in k_2 at lower temperature could be induced by reduced viscosity in the inner layer or weakened thermal motion
238 of *n*-alkane molecules (Mattila et al., 2023). It should be noted that compression of bag volume during experiment would lead
239 to an increase in the area to volume ratio. Consequently, this could disrupt the relatively slow diffusion process. Based on
240 some photos during the experiment, the leak-out air could have increased the area to volume ratio by a few factors. Further
241 research, that incorporates changes in FEP film properties with temperature would be needed in the future for quantitatively
242 interpreting the data. Further study, that incorporates considering changes of chamber volume, would be needed in the future
243 for quantitatively interpreting the data.

244 4 Conclusions

245 The present study investigated the wall loss process of C₁₄-C₁₉ *n*-alkanes to the wall of a 1 m³ chamber bag, which was
246 composed of ~~the~~ FEP film. The temperature of the chamber was controlled for the range of 262 to 298 K. Decay in gas-phase
247 concentrations of the *n*-alkanes was quantified using the SV-TAG for 15 hours following injection. The temporal variations in

248 the *n*-alkane concentrations suggested two types of loss processes. The first process was characterized by rapid exponential
249 decay in the first few hours. Subsequently, slow first-order decreases in the *n*-alkane concentrations were identified until the
250 end of the experiment. Enhanced wall loss was observed at lower temperatures for all compounds.

251 The experimental data were well fitted using the two-layer kinetic model, which considers partitioning of gas-phase
252 species to the surface layer of the chamber film and further diffusion to the inner layer. The analysis suggests that when the
253 Teflon bag chamber is operated at low temperatures, partitioning of gas phase species to the chamber wall surface is enhanced,
254 whereas the permeation of the chemical compounds to the inner layer is suppressed. The temperature effect on gas-surface
255 partitioning overweighs that on diffusion into the inner layer for *n*-alkanes, leading to an overall enhanced wall loss at lower
256 temperature.

257 The quasi-equilibrium partitioning of *n*-alkanes between the gas phase and surface layer was interpreted by considering
258 the dissolution process of the species into the surface layer. Values of $C_{surface}/C_{gas}$ at quasi-equilibrium are proportional to
259 $RT/P_s(T)$ for individual compounds. The result suggests that decreased saturation vapor pressure is the major driving force
260 for enhanced partitioning to the surface layer at low temperatures for all investigated compounds, while their activity
261 coefficients can be practically treated as constants for the investigated temperature range. The relationship can be potentially
262 employed for predicting changes in wall loss of SVOCs as a function of temperature, after further verification employing other
263 types of organic compounds.

264 In the future, the underlying mechanisms of the present findings will need to be sought for a better understanding of the
265 chamber wall loss of SVOCs. The present study focused on *n*-alkanes. In the case of chamber experiments for SOA formation,
266 wall loss processes of oxygenated chemical species would be more important. Thus, a temperature-dependent wall loss study
267 for oxygenated chemical species will still need to be conducted for interpreting SOA chamber experiments under a wide range
268 of temperatures.

269 **Data Availability**

270 Data will be made available on request.

271 **Author contribution**

272 **Longkun He:** Conceptualization, Methodology, Experiment, Data curation, Formal analysis, Writing – original draft. **Wenli**
273 **Liu:** Methodology, Experiment, Writing – review & editing. **Yatai Li:** Methodology, Writing – review & editing. **Jixuan**
274 **Wang:** Experiment, Writing – review & editing. **Mikinori Kuwata:** Conceptualization, Methodology, Project administration,

275 Funding acquisition, Formal analysis, Writing – review & editing, Supervision. **Yingjun Liu:** Conceptualization,
276 Methodology, Project administration, Funding acquisition, Formal analysis, Writing – review & editing, Supervision.

277 **Competing interests**

278 The authors declare that they have no conflict of interest.

279 **Acknowledgements**

280 We thank Dr. Ying Zhou for assisting to improve figure quality. This research was supported by the National Natural
281 Science Foundation of China (92044303, 42175121, and 42150610485).

282 **Reference**

- 283 Bunz, H., Möhler, O., Naumann, K., Saathoff, H., Schöck, W., and Schurath, U.: The novel aerosol chamber facility
284 AIDA: status and first results, Proc. 7th European Symposium on the Physico-Chemical Behaviour of Atmospheric Pollutants,
285 1996.
- 286 Clark, C. H., Kacarab, M., Nakao, S., Asa-Awuku, A., Sato, K., and Cocker, D. R., III: Temperature Effects on Secondary
287 Organic Aerosol (SOA) from the Dark Ozonolysis and Photo-Oxidation of Isoprene, Environ. Sci. Technol., 50, 5564-5571,
288 <https://doi.org/10.1021/acs.est.5b05524>, 2016.
- 289 Cocker, D. R., Flagan, R. C., and Seinfeld, J. H.: State-of-the-art chamber facility for studying atmospheric aerosol
290 chemistry, Environ. Sci. Technol., 35, 2594-2601, <https://doi.org/10.1021/es0019169>, 2001.
- 291 Compernelle, S., Ceulemans, K., and Muller, J. F.: EVAPORATION: a new vapour pressure estimation method for
292 organic molecules including non-additivity and intramolecular interactions, Atmos. Chem. Phys., 11, 9431-9450,
293 <https://doi.org/10.5194/acp-11-9431-2011>, 2011.
- 294 Deng, Y. G., Inomata, S., Sato, K., Ramasamy, S., Morino, Y., Enami, S., and Tanimoto, H.: Temperature and acidity
295 dependence of secondary organic aerosol formation from alpha-pinene ozonolysis with a compact chamber system, Atmos.
296 Chem. Phys., 21, 5983-6003, <https://doi.org/10.5194/acp-21-5983-2021>, 2021.
- 297 Hidy, G. M.: Atmospheric Chemistry in a Box or a Bag, Atmosphere, 10, <https://doi.org/10.3390/atmos10070401>, 2019.
- 298 Huang, W., Saathoff, H., Pajunoja, A., Shen, X. L., Naumann, K. H., Wagner, R., Virtanen, A., Leisner, T., and Mohr,
299 C.: alpha-Pinene secondary organic aerosol at low temperature: chemical composition and implications for particle viscosity,
300 Atmos. Chem. Phys., 18, 2883-2898, <https://doi.org/10.5194/acp-18-2883-2018>, 2018a.
- 301 Huang, Y. L., Zhao, R., Charan, S. M., Kenseth, C. M., Zhang, X., and Seinfeld, J. H.: Unified Theory of Vapor-Wall
302 Mass Transport in Teflon-Walled Environmental Chambers, Environ. Sci. Technol., 52, 2134-2142,
303 <https://doi.org/10.1021/acs.est.7b05575>, 2018b.
- 304 Isaacman, G., Kreisberg, N. M., Worton, D. R., Hering, S. V., and Goldstein, A. H.: A versatile and reproducible
305 automatic injection system for liquid standard introduction: application to in-situ calibration, Atmos. Meas. Tech., 4, 1937-
306 1942, <https://doi.org/10.5194/amt-4-1937-2011>, 2011.
- 307 Kontogeorgis, G. M., Fredenslund, A., and Tassios, D. P.: Simple Activity-Coefficient Model for The Prediction of
308 Solvent Activities in Polymer-Solutions, Ind. Eng. Chem. Res., 32, 362-372, <https://doi.org/10.1021/ie00014a013>, 1993.
- 309 Krechmer, J. E., Day, D. A., and Jimenez, J. L.: Always Lost but Never Forgotten: Gas-Phase Wall Losses Are Important
310 in All Teflon Environmental Chambers, Environ. Sci. Technol., 54, 12890-12897, <https://doi.org/10.1021/acs.est.0c03381>,
311 2020.
- 312 Krechmer, J. E., Pagonis, D., Ziemann, P. J., and Jimenez, J. L.: Quantification of Gas-Wall Partitioning in Teflon
313 Environmental Chambers Using Rapid Bursts of Low-Volatility Oxidized Species Generated in Situ, Environ. Sci. Technol.,
314 50, 5757-5765, <https://doi.org/10.1021/acs.est.6b00606>, 2016.

315 Kristensen, K., Jensen, L. N., Glasius, M., and Bilde, M.: The effect of sub-zero temperature on the formation and
316 composition of secondary organic aerosol from ozonolysis of alpha-pinene, *Environ. Sci.-Process Impacts*, 19, 1220-1234,
317 <https://doi.org/10.1039/c7em00231a>, 2017.

318 Kroll, J. H., Chan, A. W. H., Ng, N. L., Flagan, R. C., and Seinfeld, J. H.: Reactions of semivolatile organics and their
319 effects on secondary organic aerosol formation, *Environ. Sci. Technol.*, 41, 3545-3550, <https://doi.org/10.1021/es062059x>,
320 2007.

321 Li, Y. T., He, L. K., Xie, D., Zhao, A. Q., Wang, L. X., Kreisberg, N. M., Jayne, J., and Liu, Y. J.: Strong temperature
322 influence and indiscernible ventilation effect on dynamics of some semivolatile organic compounds in the indoor air of an
323 office, *Environ. Int.*, 165, <https://doi.org/10.1016/j.envint.2022.107305>, 2022a.

324 Li, Y. T., Xie, D., He, L. K., Zhao, A. Q., Wang, L. X., Kreisberg, N. M., Jayne, J., and Liu, Y. J.: Dynamics of di-2-
325 ethylhexyl phthalate (DEHP) in the indoor air of an office, *Build. Environ.*, 223,
326 <https://doi.org/10.1016/j.buildenv.2022.109446>, 2022b.

327 Matsunaga, A. and Ziemann, P. J.: Gas-Wall Partitioning of Organic Compounds in a Teflon Film Chamber and Potential
328 Effects on Reaction Product and Aerosol Yield Measurements, *Aerosol Sci. Technol.*, 44, 881-892,
329 <https://doi.org/10.1080/02786826.2010.501044>, 2010.

330 Mattila, J. M., Li, E. Y., and Offenberg, J. H.: Tubing material considerably affects measurement delays of gas-phase
331 oxygenated per- and polyfluoroalkyl substances, *J. Air Waste Manage. Assoc.*, 73, 335-344,
332 <https://doi.org/10.1080/10962247.2023.2174612>, 2023.

333 McMurry, P. H. and Grosjean, D.: Gas and Aerosol Wall Losses in Teflon Film Smog Chambers, *Environ. Sci. Technol.*,
334 19, 1176-1182, <https://doi.org/10.1021/es00142a006>, 1985.

335 Nakao, S., Shrivastava, M., Anh, N., Jung, H., and Cocker, D., III: Interpretation of Secondary Organic Aerosol Formation
336 from Diesel Exhaust Photooxidation in an Environmental Chamber, *Aerosol Sci. Technol.*, 45,
337 <https://doi.org/10.1080/02786826.2011.573510>, 2011.

338 Ng, N. L., Chhabra, P. S., Chan, A. W. H., Surratt, J. D., Kroll, J. H., Kwan, A. J., McCabe, D. C., Wennberg, P. O.,
339 Sorooshian, A., Murphy, S. M., Dalleska, N. F., Flagan, R. C., and Seinfeld, J. H.: Effect of NO_x level on secondary organic
340 aerosol (SOA) formation from the photooxidation of terpenes, *Atmos. Chem. Phys.*, 7, 5159-5174, [https://doi.org/10.5194/acp-](https://doi.org/10.5194/acp-7-5159-2007)
341 [7-5159-2007](https://doi.org/10.5194/acp-7-5159-2007), 2007.

342 Pratap, V., Bian, Q. J., Kiran, S. A., Hopke, P. K., Pierce, J. R., and Nakao, S.: Investigation of levoglucosan decay in
343 wood smoke smog-chamber experiments: The importance of aerosol loading, temperature, and vapor wall losses in interpreting
344 results, *Atmos. Environ.*, 199, 224-232, <https://doi.org/10.1016/j.atmosenv.2018.11.020>, 2019.

345 Pratap, V., Kiran, S. A., Bian, Q., Pierce, J. R., Hopke, P. K., and Nakao, S.: Observation of Vapor Wall Deposition in a
346 Smog Chamber Using Size Evolution of Pure Organic Particles, *Aerosol Air Qual. Res.*, 20, 2705-2714,
347 <https://doi.org/10.4209/aaqr.2020.05.0268>, 2020.

348 Quelever, L. L. J., Kristensen, K., Jensen, L. N., Rosati, B., Teiwes, R., Daellenbach, K. R., Perakyla, O., Roldin, P.,
349 Bossi, R., Pedersen, H. B., Glasius, M., Bilde, M., and Ehn, M.: Effect of temperature on the formation of highly oxygenated
350 organic molecules (HOMs) from alpha-pinene ozonolysis, *Atmos. Chem. Phys.*, 19, 7609-7625, [https://doi.org/10.5194/acp-](https://doi.org/10.5194/acp-19-7609-2019)
351 [19-7609-2019](https://doi.org/10.5194/acp-19-7609-2019), 2019.

352 Simon, M., Dada, L., Heinritzi, M., Scholz, W., Stolzenburg, D., Fischer, L., Wagner, A. C., Kurten, A., Rorup, B., He, X. C.,
353 Almeida, J., Baalbaki, R., Baccharini, A., Bauer, P. S., Beck, L., Bergen, A., Bianchi, F., Brakling, S., Brilke, S., Caudillo,
354 L., Chen, D. X., Chu, B. W., Dias, A., Draper, D. C., Duplissy, J., El-Haddad, I., Finkenzeller, H., Frege, C., Gonzalez-
355 Carracedo, L., Gordon, H., Granzin, M., Hakala, J., Hofbauer, V., Hoyle, C. R., Kim, C., Kong, W. M., Lamkaddam, H.,
356 Lee, C. P., Lehtipalo, K., Leiminger, M., Mai, H. J., Manninen, H. E., Marie, G., Marten, R., Mentler, B., Molteni, U.,
357 Nichman, L., Nie, W., Ojdanic, A., Onnela, A., Partoll, E., Petaja, T., Pfeifer, J., Philippov, M., Quelever, L. L. J.,
358 Ranjithkumar, A., Rissanen, M. P., Schallhart, S., Schobesberger, S., Schuchmann, S., Shen, J. L., Sipila, M., Steiner, G.,
359 Stozhkov, Y., Tauber, C., Tham, Y. J., Tome, A. R., Vazquez-Pufleau, M., Vogel, A. L., Wagner, R., Wang, M. Y., Wang,
360 D. S., Wang, Y. H., Weber, S. K., Wu, Y. S., Xiao, M., Yan, C., Ye, P. L., Ye, Q., Zauner-Wieczorek, M., Zhou, X. Q.,
361 Baltensperger, U., Dommen, J., Flagan, R. C., Hansel, A., Kulmala, M., Volkamer, R., Winkler, P. M., Worsnop, D. R.,
362 Donahue, N. M., Kirkby, J., and Curtius, J.: Molecular understanding of new-particle formation from alpha-pinene
363 between-50 and+25 degrees C, *Atmos. Chem. Phys.*, 20, 9183-9207, <https://doi.org/10.5194/acp-20-9183-2020>, 2020.

364 Song, C., Na, K. S., and Cocker, D. R.: Impact of the hydrocarbon to NOx ratio on secondary organic aerosol formation,
365 *Environ. Sci. Technol.*, 39, 3143-3149, <https://doi.org/10.1021/es0493244>, 2005.

366 Voigtlaeander, J., Duplissy, J., Rondo, L., Kuerten, A., and Stratmann, F.: Numerical simulations of mixing conditions
367 and aerosol dynamics in the CERN CLOUD chamber, *Atmos. Chem. Phys.*, 12, 2205-2214, [https://doi.org/10.5194/acp-12-](https://doi.org/10.5194/acp-12-2205-2012)
368 [2205-2012](https://doi.org/10.5194/acp-12-2205-2012), 2012.

369 Wang, M. Y., Xiao, M., Bertozzi, B., Marie, G., Rorup, B., Schulze, B., Bardakov, R., He, X. C., Shen, J. L., Scholz, W.,
370 Marten, R., Dada, L., Baalbaki, R., Lopez, B., Lamkaddam, H., Manninen, H. E., Amorim, A., Ataei, F., Bogert, P., Brasseur,
371 Z., Caudillo, L., De Menezes, L. P., Duplissy, J., Ekman, A. M. L., Finkenzeller, H., Carracedo, L. G., Granzin, M., Guida, R.,
372 Heinritzi, M., Hofbauer, V., Hohler, K., Korhonen, K., Krechmer, J. E., Kurten, A., Lehtipalo, K., Mahfouz, N. G. A.,
373 Makhmutov, V., Massabo, D., Mathot, S., Mauldin, R. L., Mentler, B., Muller, T., Onnela, A., Petaja, T., Philippov, M.,
374 Piedehierro, A. A., Pozzer, A., Ranjithkumar, A., Schervish, M., Schobesberger, S., Simon, M., Stozhkov, Y., Tome, A., Umo,
375 N. S., Vogel, F., Wagner, R., Wang, D. S., Weber, S. K., Welti, A., Wu, Y. S., Zauner-Wieczorek, M., Sipila, M., Winkler, P.
376 M., Hansel, A., Baltensperger, U., Kulmala, M., Flagan, R. C., Curtius, J., Riipinen, I., Gordon, H., Lelieveld, J., El-Haddad,
377 I., Volkamer, R., Worsnop, D. R., Christoudias, T., Kirkby, J., Mohler, O., and Donahue, N. M.: Synergistic HNO3-H2SO4-
378 NH3 upper tropospheric particle formation, *Nature*, 605, 483-+, <https://doi.org/10.1038/s41586-022-04605-4>, 2022.

379 Yeh, G. K. and Ziemann, P. J.: Alkyl Nitrate Formation from the Reactions of C-8-C-14 n-Alkanes with OH Radicals in
380 the Presence of NOx: Measured Yields with Essential Corrections for Gas-Wall Partitioning, *J. Phys. Chem. A*, 118, 8147-
381 8157, <https://doi.org/10.1021/jp500631v>, 2014.

382 Yeh, G. K. and Ziemann, P. J.: Gas-Wall Partitioning of Oxygenated Organic Compounds: Measurements, Structure-
383 Activity Relationships, and Correlation with Gas Chromatographic Retention Factor, *Aerosol Sci. Technol.*, 49, 726-737,
384 <https://doi.org/10.1080/02786826.2015.1068427>, 2015.

385 Yu, S., Jia, L., Xu, Y., Zhang, H., Zhang, Q., and Pan, Y.: Wall losses of oxygenated volatile organic compounds from
386 oxidation of toluene: Effects of chamber volume and relative humidity *, *J. Environ. Sci.*, 114, 475-484,
387 <https://doi.org/10.1016/j.jes.2021.09.026>, 2022.

388 Zhang, X., Cappa, C. D., Jathar, S. H., McVay, R. C., Ensberg, J. J., Kleeman, M. J., and Seinfeld, J. H.: Influence of
389 vapor wall loss in laboratory chambers on yields of secondary organic aerosol, *Proc. Natl. Acad. Sci. U. S. A.*, 111, 5802-5807,
390 <https://doi.org/10.1073/pnas.1404727111>, 2014.

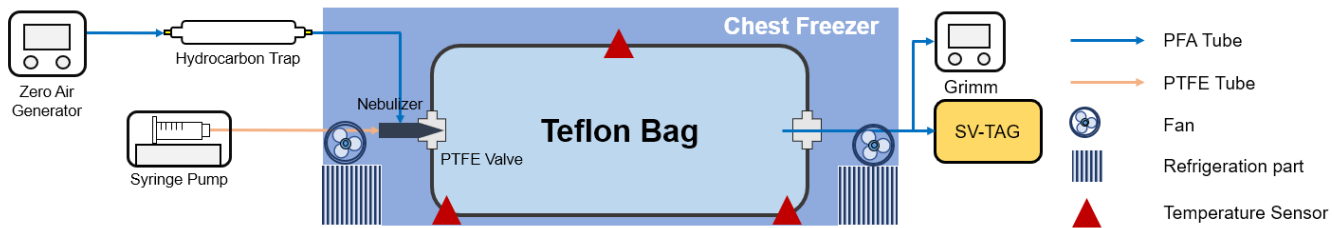
391 Zhang, X., Schwantes, R. H., McVay, R. C., Lignell, H., Coggon, M. M., Flagan, R. C., and Seinfeld, J. H.: Vapor wall
392 deposition in Teflon chambers, *Atmos. Chem. Phys.*, 15, 4197-4214, <https://doi.org/10.5194/acp-15-4197-2015>, 2015.

393 Zhao, Y. L., Kreisberg, N. M., Worton, D. R., Teng, A. P., Hering, S. V., and Goldstein, A. H.: Development of an In
394 Situ Thermal Desorption Gas Chromatography Instrument for Quantifying Atmospheric Semi-Volatile Organic Compounds,
395 *Aerosol Sci. Technol.*, 47, 258-266, <https://doi.org/10.1080/02786826.2012.747673>, 2013.

396 Nomenclature

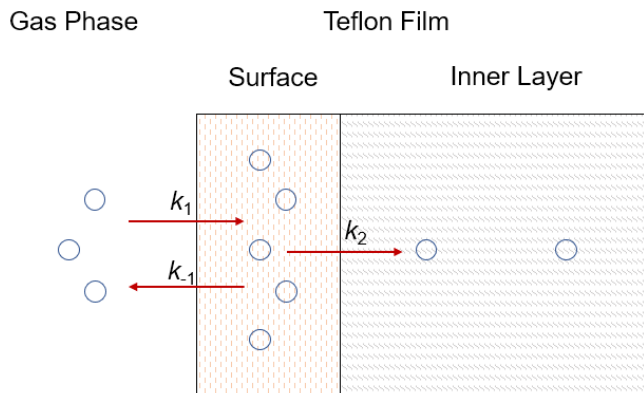
397 A table that contains the definitions of parameters and corresponding units.

398	k_1	forward rate constant (mins^{-1})
399	k_{-1}	backward rate constant (mins^{-1})
400	k_2	first-order loss rate constant (mins^{-1})
401	$\tau_{surface}$	gas-surface equilibrium time scale (min)
402	τ_{inner}	diffusion time scale (min)
403	C_0	initial SVOC concentration in gas phase ($\mu\text{g m}^{-3}$)
404	C_{gas}	SVOC concentration in gas phase ($\mu\text{g m}^{-3}$)
405	C_{wall}	SVOC concentration on wall surface ($\mu\text{g m}^{-3}$)
406	K_{eq}	gas-surface equilibrium constant
407	$C_{FEP_surface}$	equivalent organic mass concentration of the FEP chamber surface (mg m^{-3})
408	M_{wall}	average molecular mass of the Teflon wall (g mol^{-1})
409	$\gamma_{FEP_surface}$	activity coefficient in the Teflon surface
410	R	gas constant ($\text{J K}^{-1} \text{mol}^{-1}$)
411	T	temperature (K)
412	$P_s(T)$	saturation vapor pressure of compound at temperature T (Pa)



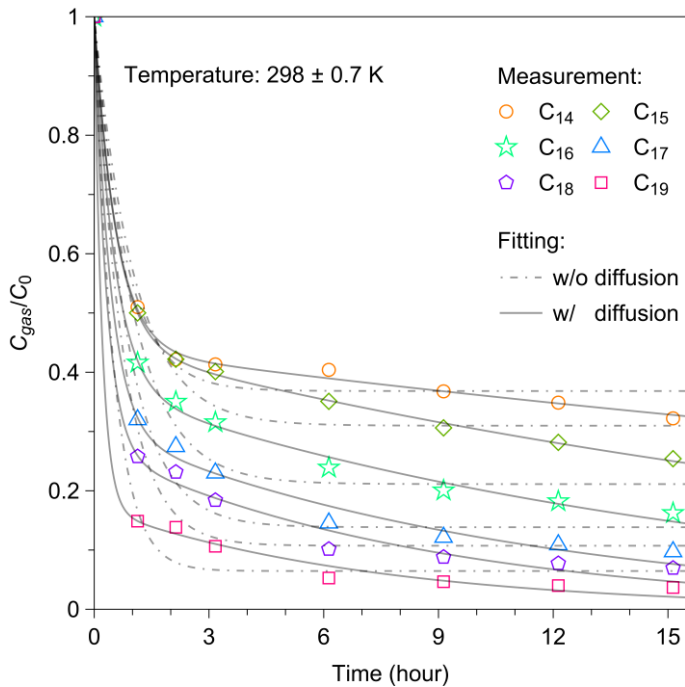
413

414 **Figure 1.** Schematic diagram of the experimental setup.



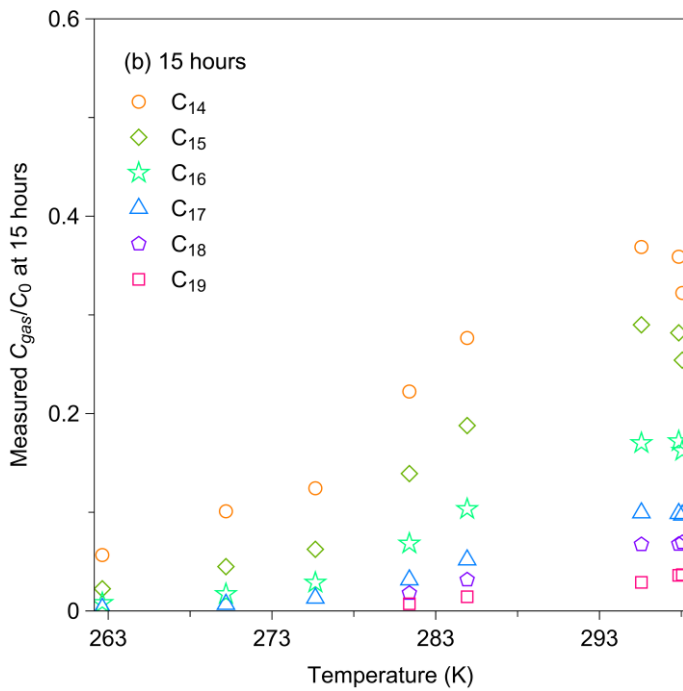
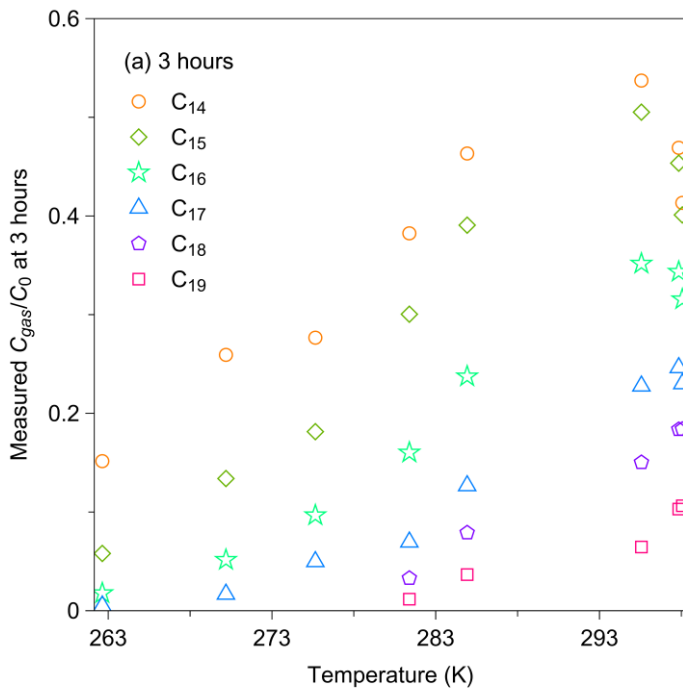
415

416 **Figure 2.** Schematic diagram of wall loss process. Compounds partition between gas phase and surface layer with forward
417 and backward rates (k_1 and k_{-1}). Compounds in surface layer undergo irreversible diffusion into inner layer with first-order
418 loss rate (k_2).



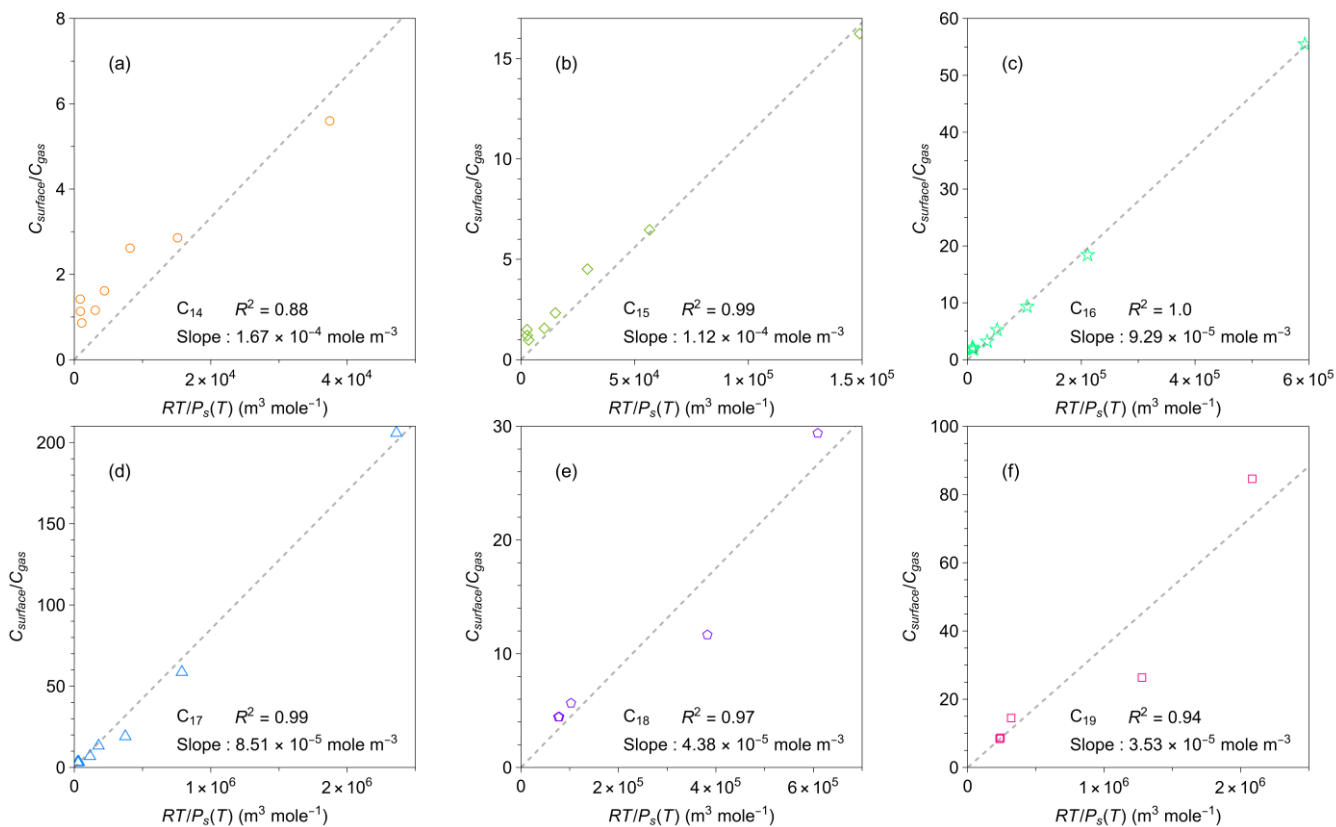
419

420 **Figure 3.** Temporal variation in C_{gas}/C_0 for C₁₄-C₁₉ *n*-alkanes at 298 ± 0.7 K following injection. C_{gas} is the concentration of
 421 each *n*-alkane in the gas phase, and C_0 is the corresponding initial concentration of each *n*-alkane. The two-layer kinetic
 422 sorption model (Section 2.2) was employed to fit the data (black solid line). The black dot-dashed lines show the fitting result
 423 to the model that ignores the diffusion process to the inner layer (*i.e.*, $k_2 = 0$).



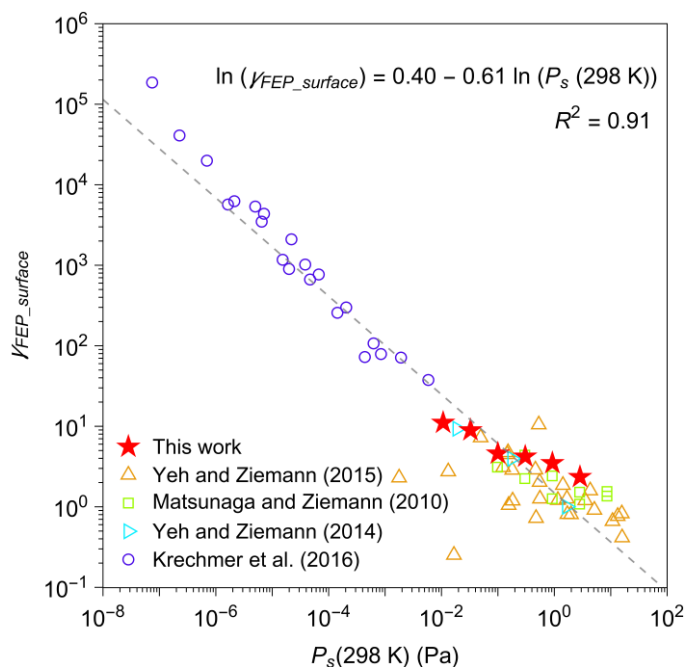
424

425 **Figure 4.** Measured values of C_{gas}/C_0 at (a) 3 hours and (b) 15 hours after injection.



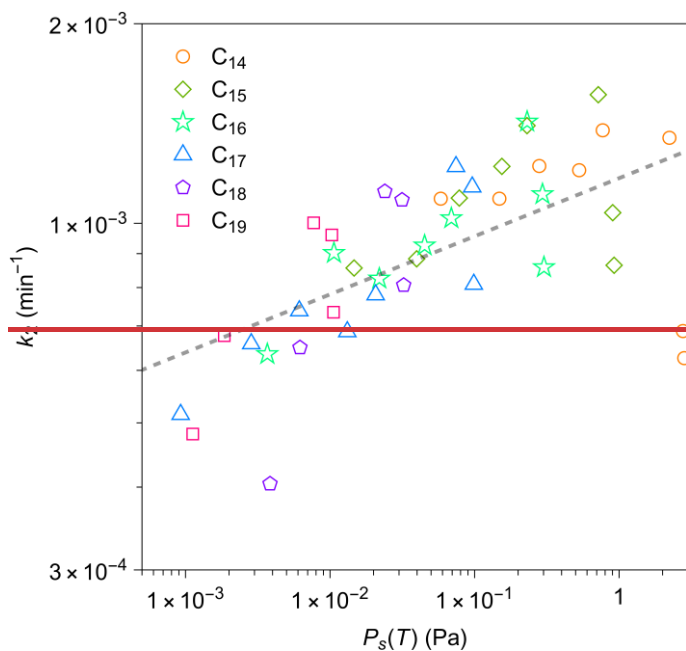
426

427 **Figure 5.** Relationships between measured ratio of concentrations in the chamber wall surface phase and in the gas phase at
 428 quasi-equilibrium and calculated values of $RT/P_s(T)$ for individual n -alkanes. Calculation methods for $C_{surface}/C_{gas}$ is
 429 detailed in the text. The values of $RT/P_s(T)$ for each n -alkane were calculated by the EVAPORATION group contribution
 430 method (Compennolle et al., 2011). The black dashed lines are linear least-squares that fit the data for each n -alkane.

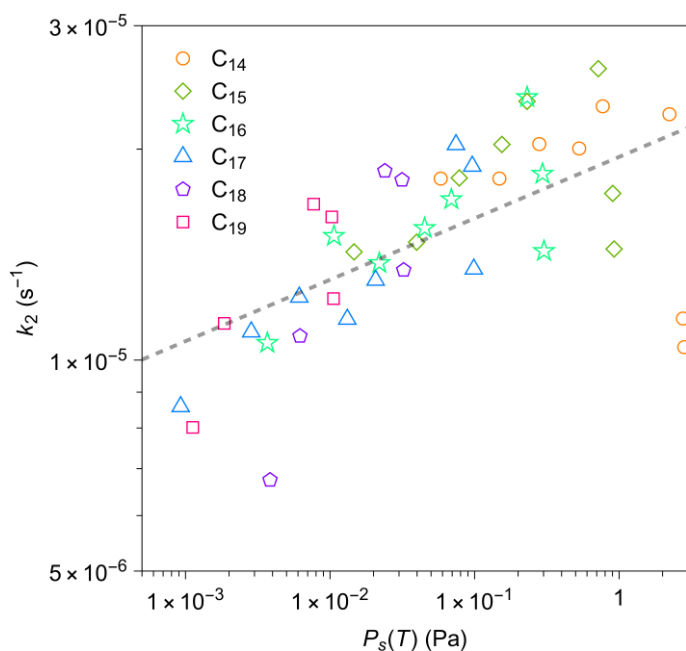


431

432 **Figure 6.** Activity coefficient ($\gamma_{FEP_surface}$) of organic compounds in FEP film. The sources of data include this work and the
 433 literature (compiled by Huang et al. (2018b), including Matsunaga and Ziemann (2010), Yeh and Ziemann (2014, 2015), and
 434 Krechmer et al. (2016)) (~~Matsunaga and Ziemann, 2010; Yeh and Ziemann, 2014, 2015; Krechmer et al., 2016~~). A list of
 435 chemical species that were investigated by each study is available in Table S4. Saturation vapor pressures at 298 K ($P_s(298\text{ K})$)
 436 were estimated by EVAPORATION (Compernelle et al., 2011).



437



438

439 **Figure 7.** Relationship between calculated first-order loss rate k_2 for each n -alkane and calculated values of saturation vapor
 440 pressure by the EVAPORATION group contribution method (Compernelle et al., 2011). The calculation method for k_2 is
 441 detailed in the text. The black dashed line is a linear least-squares fit to the data in a logarithmic scale.